Contract No.:

This manuscript has been authored by Savannah River Nuclear Solutions (SRNS), LLC under Contract No. DE-AC09-08SR22470 with the U.S. Department of Energy (DOE) Office of Environmental Management (EM).

Arrays of Position-Sensitive Virtual Frisch-Grid CdZnTe Detectors: Results from a 4x4 array prototype

L. Ocampo Giraldo, *Member IEEE,* A. E. Bolotnikov, *Member IEEE,* G. S. Camarda, *Member IEEE,* S. Cheng, G. De Geronimo, *Member IEEE,* A. McGilloway, J. Fried, D. Hodges, A. Hossain, *Member IEEE,* K. Ünlü, M. Petryk, V. Vidal, E. Vernon, G. Yang, *Member IEEE* and R. B. James, *Fellow IEEE*

***Abstract*—Position-sensitive virtual Frisch-grid CdZnTe (CZT) detectors offers a unique capability for correcting the response non-uniformities caused by crystal defects. This allowed us to achieve high-energy resolution, while using typical-grade commercial CZT crystals with relaxed requirements to their quality, thus reducing the overall cost of detectors. Another advantage of the virtual Frisch-grid detectors is that they can be integrated into arrays and used in small compact hand-held instruments or large-area gamma cameras that will enhance detection capability for many practical applications, including nonproliferation, medical imaging and gamma-ray astronomy. Here, we present the results from testing small array prototypes coupled with front-end ASIC. Each detector in the array is furnished with 5 mm-wide charge-sensing pads placed near the anode. The pads signals are converted into X-Y coordinates, which combined with the cathode signals (for Z coordinates), provide 3D position information of all interaction points. The basic array consists of a number of detectors grouped into 2x2 sub-arrays, each having a common cathode made by connecting together the cathodes of the individual detectors. These features can significantly improve the performance of detectors while using typical-grade low cost CZT crystals to reduce the overall cost of the proposed instrument.**

***Index Terms*—CdZnTe, high-granularity detectors, 3D position-sensitive virtual Frisch-grid detectors, crystal defects, charge-loss correction**

I. Introduction

Position-sensitive virtual Frisch-grid (VFG) CdZnTe (CZT) detectors have been demonstrated to provide high detection efficiency, high energy resolution and a capability to correct response non-uniformity caused by crystal defects [1,2]. This allows us to make high spectroscopic performance gamma-ray detectors while using standard-grade (unselected) commercial CZT crystals with relaxed material requirements, which helps to reduce the cost of the detectors. The VFG detectors employ a small area, ~6x6 mm^2, but long, up to 5 cm, CZT crystals (bars) that have much higher production-yield and lower cost than crystals used for large pixelated detectors. The high geometrical aspect ratio and the charge-sensing pads near the anode produce the effect as if a real Frisch-grid was used to electrostatically shield the anode from the positive holes.

The virtual Frisch-grid design was originally proposed for a noble gas ionization chamber with a long drift region [3]. This design approach turned out to be more beneficial for CZT detectors and was used in CAPture™ [4], hemispherical [5], Frisch-ring [6], and capacitive Frisch-grid [7] detectors.

In our detectors, 4 non-contacting position-sensing pads are attached to the side surfaces near the anode. These non-contacting electrodes are similar to those used in capacitive Frisch-grid [6] and Frisch-ring [7] detectors. The amplitudes of the signals readout from the strips are used to evaluate X-Y coordinates, while the drift time and the cathode-to-anode ratio, C/A, were used to independently evaluate the Z coordinate for the location of each interaction point. Virtually grounded pads produce the Frisch-grid effect, as if a real grid was placed inside the detector.

Previously, we demonstrated that position-sensitive VFG detectors could be made with thicknesses up to 50 mm [2]. Arrays of such detectors can be used in compact hand-held instruments or large-area gamma cameras for spectroscopy and imaging of gamma-ray sources.

In this work, we tested design approaches and performance of 4x4 array prototypes coupled with the front-end ASIC and evaluated the energy and position resolutions.

II. Array design

We used a modular approach with a design that would allow for easy replacement of individual detectors. The baseline module (Fig. 1) consists of the detector board carrying 6x6x20 mm^3 detectors, which are slid inside the 5-mm-deep cells of a honeycomb holder. Its walls are comprised of crisscrossing 5-mm wide and 0.5-mm thick strips, cut from a PC board, with a set of narrow spring-strip contacts used to provide connections to the pads. Additionally, a 1-mm thin plastic grid is used to hold the detectors in place.

Each crystal is encapsulated inside the ultra-thin polyester shell for electrical insulation and mechanical protection of the

The work was supported by the Office of Nonproliferation and International Security, Office of Nuclear Safeguards & Security, Next Generation Safeguards Initiative's Safeguards Technology Development Team, and the work to develop CZT detectors with thickness up to 50 mm was supported by the U.S. Department of Energy, Office of Defense Nuclear Nonproliferation Research & Development.The manuscript has been authored by Brookhaven Science Associates, LLC under Contract No. DE-AC02-98CH1-886 with the U.S. Department of Energy.

L. Ocampo Giraldo and K. Ünlü are with Mechanical and Nuclear Engineering Department, Pennsylvania State University, University Park, PA16802 (phone: 631-344-8364; e-mail: lio5000@psu.edu).

A. E. Bolotnikov, G. S. Camarda, S. Cheng, G. De Geronimo, A. McGilloway, J. Fried, A. Hossain, M. Petryk, E. Vernon, and G. Yang are with Brookhaven National Laboratory, Upton, NY 11793, USA.

D. Hodges and V. Vidal are University of Texas at El Paso, El Paso, TX 79968, USA

R. B. James was with Brookhaven National Laboratory; he is now with Savannah River National Laboratory, Aiken, SC 29803, USA.

detector's side surface. The shell also holds in place two CuBe spring contacts on the cathode and the anode faces. 5x5 mm^2 pads, cut from aluminum adhesive foil, are glued over the shell near the anodes (Fig. 1). The detectors are gently pressed to the detector board from the top using another (cathode) board having the decoupling capacitors and resistors as in the first approach. The anode spring contacts touch the designated anode pads on the board.

In this design, the detectors are held in places while the spring contacts provide reliable connections with substrate pads and protect the detectors from any mechanical and temperature shocks. The main advantage of using spring contacts is that individual detectors can be easily replaced if necessary.

The detector board is connected via multi-pin connectors located on the back of the fan-out substrate and the front side of the ASIC board. The backside of the ASIC board has two additional multi-pin connectors that are used for plugging the array modules into the readout motherboard. The current array module is designed to accommodate 16 detectors, divided into 2x2 sub-arrays of 2x2 detectors with common cathodes (see Fig. 2).

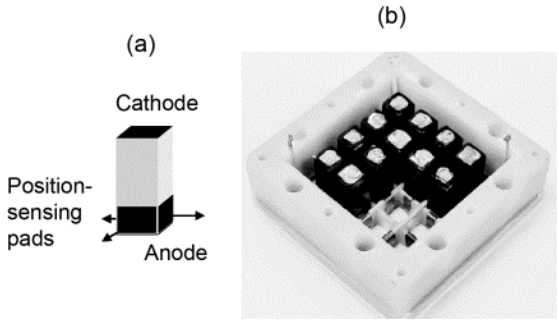

Fig. 1. (a) Schematic of the position-sensitive VFG detector. (b) The detector holder with a partially assembled array module.

From the design point of view, it is beneficial to connect together the pads of adjacent detectors facing each other in the array. We also connected adjacent pads of the peripheral detectors. This reduces a number of the required readout channels, but it creates signal ambiguity when multiple interactions occur in adjacent detectors. In such cases, we cannot use the pads with signals generated by electron clouds in two adjacent but different detectors. But the remaining signals from two orthogonal or three pads still can be used to evaluate the positions of the interaction points. We verified experimentally that two signals from two orthogonal pads are sufficient to locate the interaction point within a detector. Thus, depending on the multiplicity of the interaction events, we will use the signals from 2, 3, or 4 sensing pads to evaluate the coordinates and apply corrections. Accordingly, we use the correction matrixes evaluated for all these cases.

For testing the arrays we used detectors acquired from two vendors, eV Products and Redlen Technologies, with the same specifications for dimensions and quality.

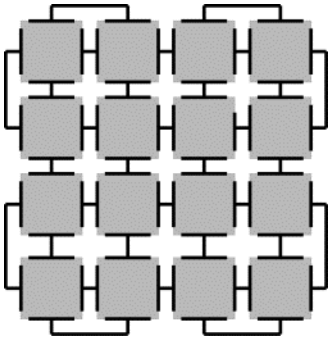

Fig. 2. Connecting the position sensing pads. The full array requires 16 anodes, 36 position-sensing pads, and 4 cathode readout channels.

For testing the arrays we took advantage of the existing front-end AVG1 ASIC developed for arrays of conventional VFG detectors without position sensing capabilities [8]. The ASIC has 36 anode and 9 cathode inputs and mimics the design of its predecessor, the H3D ASIC, developed for 3D position-sensitive pixelated detectors by BNL's Instrumentation Division in collaboration with the University of Michigan [9-11]. The anode channels implement the conventional processing chain of analog signals, including a low-noise charge-sensitive amplifier optimized for 3.3-pF input capacitance with continuous reset, a baseline stabilizer, a fifth-order unipolar shaping amplifier with an adjustable peaking time, and two peak and timing detectors for measuring the amplitude and timing for both the positive and negative pulses. Similarly, the cathode channel implements a charge-sensitive amplifier optimized for a ~ 6.3 pF input capacitance with continuous reset and a baseline stabilizer. It is followed by two parallel filtering circuits: one (with a long shaping time) for measuring the amplitude, and the other (with a short shaping time) for measuring the timing. The timing assigned to the anode signals is measured at their peaking time which is, to a first order, independent of the signal amplitude.

We employed the AVG1 ASIC for testing the 4x4 arrays as a temporary solution, because it could accommodate only 12 position-sensitive VFG detectors (not 36 as in the case of the conventional VFG detectors without position sensing). The second drawback of using the AVG1 ASIC is that it is not optimal for processing the pad signals, since it has a limited dynamic range for measuring negative amplitudes, while the electron clouds generate bipolar signals (after unipolar shaping) on the pads with the negative amplitudes being used to evaluate the X-Y coordinates. Thus, we tested the partially assembled arrays consisting of 12 detectors; 12 anode inputs were used to capture the positive amplitudes from 12 detector anodes, while the remaining 24 inputs were used to capture the negative amplitudes from the pads. The 3 cathode inputs were connected to the common cathodes of the 3 groups of 2x2 detectors. It is important to keep in mind that the AVG1 ASIC was designed for different applications and is not optimal for VFG detector arrays.

III. Testing Arrays

The array under test was plugged into a motherboard enclosed inside a metal box. The motherboard also carries the low-voltage converters supplying power to the ASIC chips, two analog-to-digital converters for digitizing the peak amplitudes and timing information from all channels, the Field Programmable Gate Array for processing the data and communicating with the ASICs and the USB port. During the measurements we placed the text box inside an environmental chamber to maintain the detectors' temperature at 17-18 ºC. Without cooling, the ASIC generates enough heat to raise the temperature inside the box up to 40 ºC. We used uncollimated ^{137}Cs, ^{133}Ba, and ^{241}Am sources normally placed ~2 cm above the cathodes to generate signals inside the detectors. The cathode's bias was set at 2500-3000 V. The electronic noise was measured at high voltage on the cathode using the test-pulse signals. The FWHMs of the test-pulse peaks were in the range of 3.2-3.5 keV, which is equivalent to 0.5-0.6% at 662 keV.

Any detector from the array could initiate the readout sequence from all channels. For each interaction event, the ASIC provides the peaks' amplitudes (positive and negative) and the corresponding times captured in all detectors. The data were saved in the computer's memory and processed off-line.

The ratio of the cathode-to-anode signals is used to evaluate the depth of the interaction point with respect to the anode, while the difference between the cathode- and anode-times gives the electron clouds' drift time after subtracting the time offsets. Both the timing and the interaction depth information can be used to apply the charge-loss correction; however, we found that reliance on the timing normally gives better performance. There is a small probability of multiple interactions occurring within a single detector; in such cases, the ASIC reports the averaged amplitude and time as if a single interaction were detected therein. In most cases we can identify such events [12].

Using the position information, we virtually divide each detector volume into small voxels and correct responses measured from each of them by using a 3-dimensional correction matrix generated during calibration [2].

A. Spectroscopic performance

Fig. 3 illustrates the performance of a 20-mm thick position-sensitive VFG detector before (left) and after (right) X-Y corrections measured with uncollimated ^{137}Cs, ^{60}Co, and ^{133}Ba sources. We applied the drift-time (or interaction depth) corrections to the spectra shown on the left.

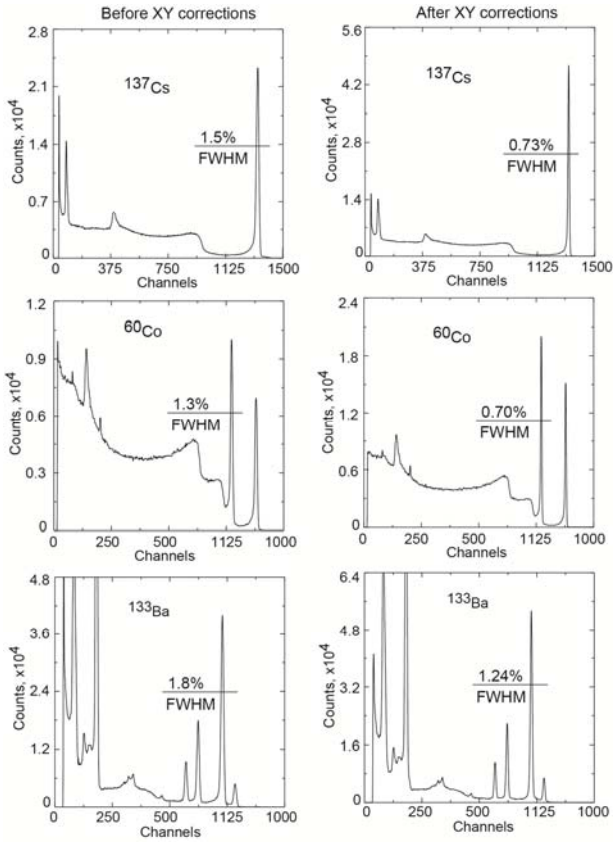

Fig. 3. Performance improvements of a 20-mm thick position-sensitive virtual Frisch-grid detector before and after corrections for three gamma-ray emitting sources.

Due to the large size of the anode, the main factor limiting the energy resolution of the position-sensitive VFG detectors is electronic noise related to the high leakage current and large anode capacitance. Fig. 4 depicts the temperature dependence of the energy resolution evaluated for one of the detectors biased at 3000 V. As seen, the detector's energy resolution stays below 1% FWHM at 662 keV for temperatures up to 35 ºC.

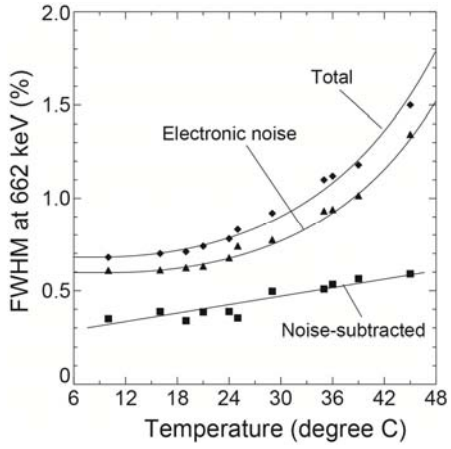

Fig. 4. Temperature dependence of the energy resolution of the 6x6x20 mm^3 detector plus ASIC (after 3D corrections). The applied voltage bias is 3000 V.

An edge effect can be a potential problem related to long-drift distance detectors. Fortunately, the naturally formed electric field inside virtual Frisch-grid detectors tends to be focused towards the central portion of the anode (i.e., away from the side walls). We observed this effect for the majority of the tested detectors; it is particularly true in the case of 20- and 25-mm long crystals. Indeed, due to the charging of deep levels, the strength of the electric field inside CZT detectors gradually decreases towards the anode, while on the surface it is more uniform due to higher surface leakage current. As a result, the electric field is naturally slightly focused towards the anode. The only exception is for crystals that contain big extended defects, such as twins or subgrain boundaries. In such cases, it is hard to predict the electric-field distribution inside the detectors due to space-charge buildup. It could be tilted towards one side of the crystal, or it could "defocus" near the anode. In both cases, some fraction of the charge will reach the side surfaces instead of the collecting electrode, resulting in incomplete charge-collection events.

We also found that if the 3D corrections are applied then we can operate detectors at reduced cathode biases. Fig. 5 shows the dependence of the energy resolution measured for a Redlen 6x6x20 mm^3 detector at different cathode bias voltages. As seen, the resolution (after corrections) remains unchanged for bias voltages as low as 1000 V. However, this does not mean that we should use such a low bias but instead the proposed detectors, 20-25 mm thick, can be operated in the range of 2000-3000 V, which is beneficial from the instrument design standpoint. For comparison, Fig. 5 also shows the photopeak width after the drift-time corrections, which correct both the charge-losses along Z, non-uniformity of the VFG detector response function, and ballistic deficit. We used a 2-μs peaking time for the ASIC's shaping amplifier.

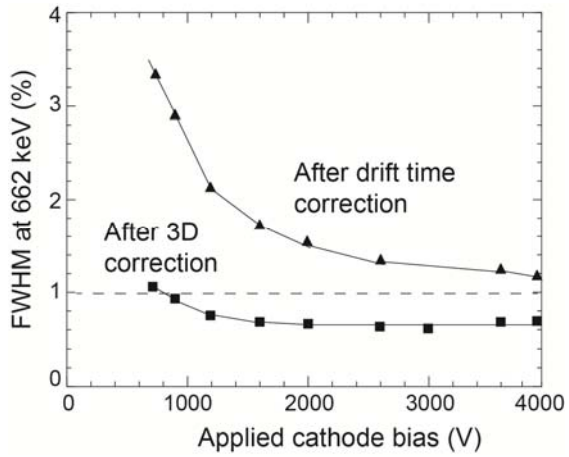

Fig. 5. The dependence of the energy resolution on the cathode bias for a 6x6x20 mm^3 detector.

Fig. 6 shows the pulse-height spectra measured from the 12-detector array before and after applying corrections using 4, 3, and 2 sensing pads, respectively. These measurements demonstrate the feasibility of our approach to the array design and signal substitution. Meaning that signals from 2 or 3 pads can substitute 4-pad signal processing in the cases of ambiguity caused by two or more Compton scattering events taking place in adjacent detectors, which prevent us from using signals from 4 pads.

It is worth mentioning that we correlated the captured anode signals with the normalized pad signals (ratios between pads and anode amplitudes), which in turn correlate to the geometrical locations of the interaction points. For correcting the responses we do not need to know the actual positions of the interaction points. The corrections are applied directly in the pad amplitude configuration space. In the next paragraph we will discuss the relations between the pad amplitudes and the actual coordinates.

B. Position sensitivity

As mentioned before, the spectral response corrections can be applied directly operating in the pad signal configuration space. However, to evaluate the actual *X*-*Y* locations of the interaction point inside the detector one has to take into account the pads response functions.

Fig. 7 illustrates the coordinate system associated with the position-sensitive VFG detector. The pad response function gives the amplitude of the pad signal versus the *X*-*Y* coordinates of the electron cloud:

$$A = R(x, y). \tag{1}$$

The inverse response function allows us to evaluate X and Y coordinates. To simplify the problem we assume that two amplitudes from the opposite pads define the position of the line along which the location of the electron cloud as determined by the two amplitudes from the orthogonal pads. For example, if the position of the line along the *X*-axis is defined by A_y^1 and A_y^2 amplitudes, then we can have two estimates for *X* each depends on A_x^1 and A_x^2:

$$X_1 = R^{-1}\left(A_x^1, A_y^1, A_y^2\right) \tag{2}$$

$$X_2 = L - R^{-1}\left(A_x^2, A_y^1, A_y^2\right), \tag{3}$$

where L is a distance between two opposite pads. Combing both estimates we can write:

$$X = \frac{X_1 W_1 + X_2 W_2}{W_1 + W_2}, \tag{4}$$

where W_1 and W_2 are the weights defined as:

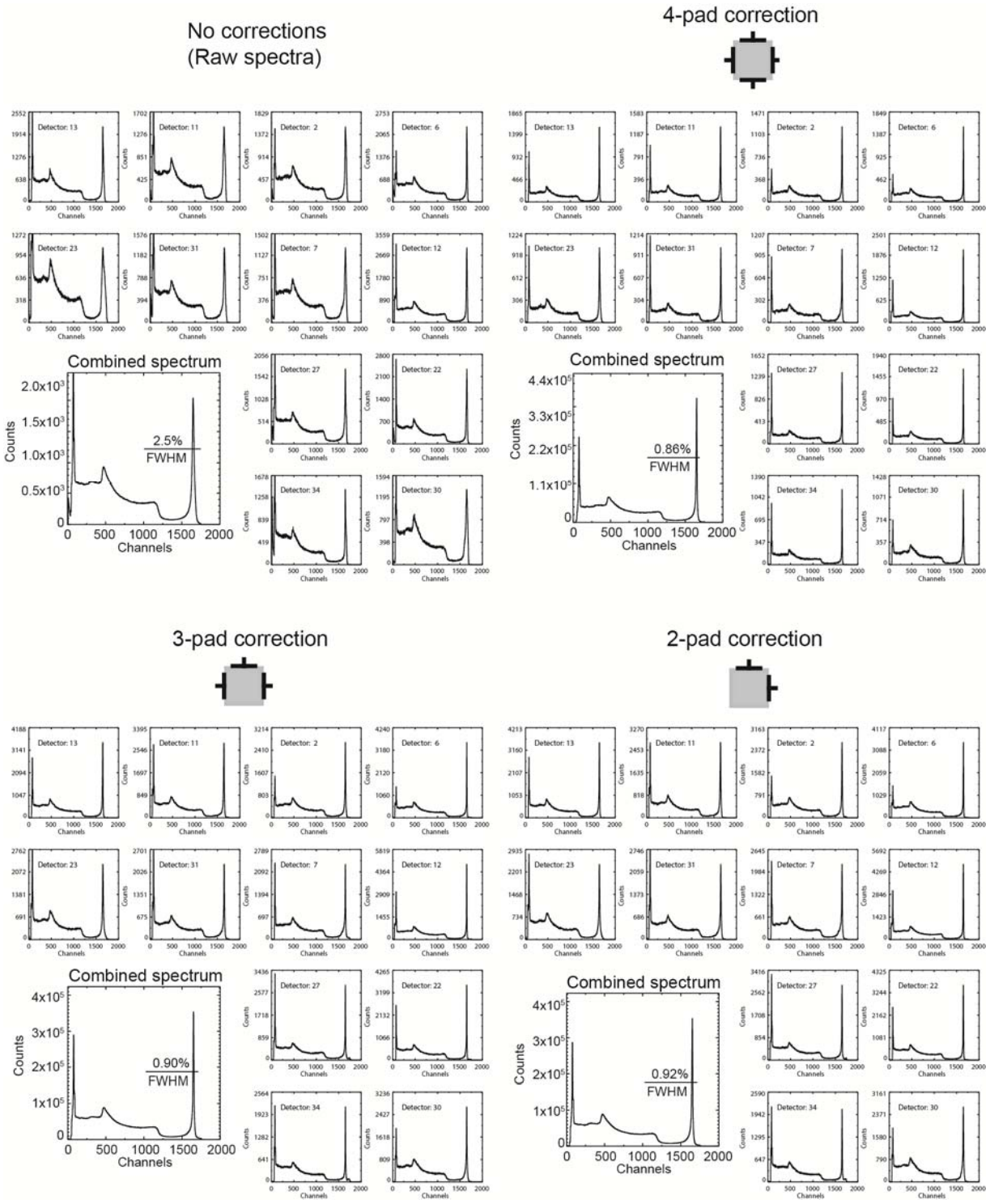

Fig. 6. Pulse-height spectra measured with the 12-detector array before and after 3D corrections using 4, 3, and 2 position sensing pads.

$$W = \frac{1}{\sigma_x^2}, \quad (5)$$

where σ_x^2 is the standard deviation of the estimates:

$$\sigma_x^2 = \left(\frac{\partial R}{\partial A}\right)^2 \sigma_A^2. \quad (6)$$

The pad response functions have to be evaluated during the calibrations. Ideally they should be identical for all detectors and all pads. The above equations can be applied in the cases of using only 2- and 3-pad signals. Using a linear approximation for the response functions and taking the signal amplitudes as the widths, we can use a first-order estimate for *X* and *Y* coordinates:

$$X = \frac{A_x^1}{A_x^1 + A_x^2} \quad (7)$$

and

$$Y = \frac{A_y^1}{A_y^1 + A_y^2}. \quad (8)$$

The first order estimates can be used for correcting the response non-uniformity, but they cause significant distortions when used for evaluating the actual coordinates, especially in the case of 2- and 3-pad signals.

To accurately evaluate the response functions, we took the measurements with an uncollimated ^{137}Cs source and tabulated the *X*-*Y* dependencies of the response functions. For *X* and *Y* we used the first-order approximations defined by Eqs. (7) and (8). Fig. 7 shows data points and a fitting curve representing changes of the response function as the location of the electron cloud moves along a direction parallel to *X* (or *Y*) axis. In this case, the dots were selected within a narrow region around a central axis of the detector. A solid line symmetrically located on the top represents the inverse response function. For comparison, a solid line on the bottom is the response function evaluated along a line near the edge of the detector. The evaluated response functions (second-order approximations) could be plugged back to evaluate the third-order approximation and so on. We found that the second- and third-order approximations have small differences, and the second-order approximation is sufficient for the *X*-*Y* coordinate evaluations.

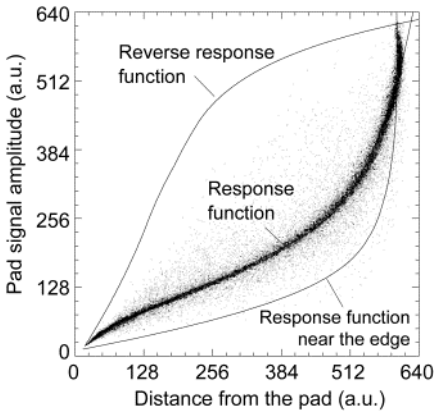

Fig. 7. 1-dimensional response function (dependence along the distance from the pad).

To illustrate an improvement in coordinate reconstruction, we plotted distributions of the locations of the interaction points and anode signal amplitudes generated by the uncollimated ^{137}Cs source. Fig. 8 (a,b) compares 2D distributions of the photoabsorption events (counts) projected onto the X-Y plane evaluated for a representative detector using the linear (a) and second-order (b) approximations for the pads response functions. 9 maps from each group correspond to using different combinations of the signal amplitudes captured from the 4 pads. The specific pads whose signals were used to reconstruct the even locations are indicated in each map. As seen from Fig. 8 (a), the linear approximation results in geometrical distortion when 2- or 3-pad signals are used. The distortion can be corrected if the second-order approximation for the pad response functions is used as illustrated in Fig. 8 (b). The last plots in each group show 1D distributions of the count across the center of the detector area. The peaks near the detector edges are due to the errors in the evaluated response functions when the electron cloud is too close to the pad. We are currently working on improving our algorithm for the response function evaluation.

To demonstrate the high imaging capability of the detector, Fig. 9 (a,b) presents 2D distributions of the anode signal amplitudes (response functions) corresponding to the 662-keV photoabsorption events. Similarly to the counts distributions above, Fig. 9 (a) shows the distorted response maps when less than 4-pad signals are used that can be corrected using the second-order approximations as shown in Fig. 9 (b). The important feature in the distributions of Fig. 9 is that crystal defects (prismatic dislocations) are clearly seen in all measurements. In the case of a linear approximation, the locations of these defects changed when less than 4-pad signals were used. In contrast, their positions are the same in all maps generated using the second-order approximations (Fig 9. (b)). Also, taking into account that the total map area is 6x6 mm^2, we could estimate the size of the smallest feature to be less than 0.5 mm. This gives a good estimate for the *absolute* position resolution of the VFG detector with the charge-sensing pads. We note that the *local* position resolution is significantly better, ~100 μm, which is critical for the charge-loss correction.

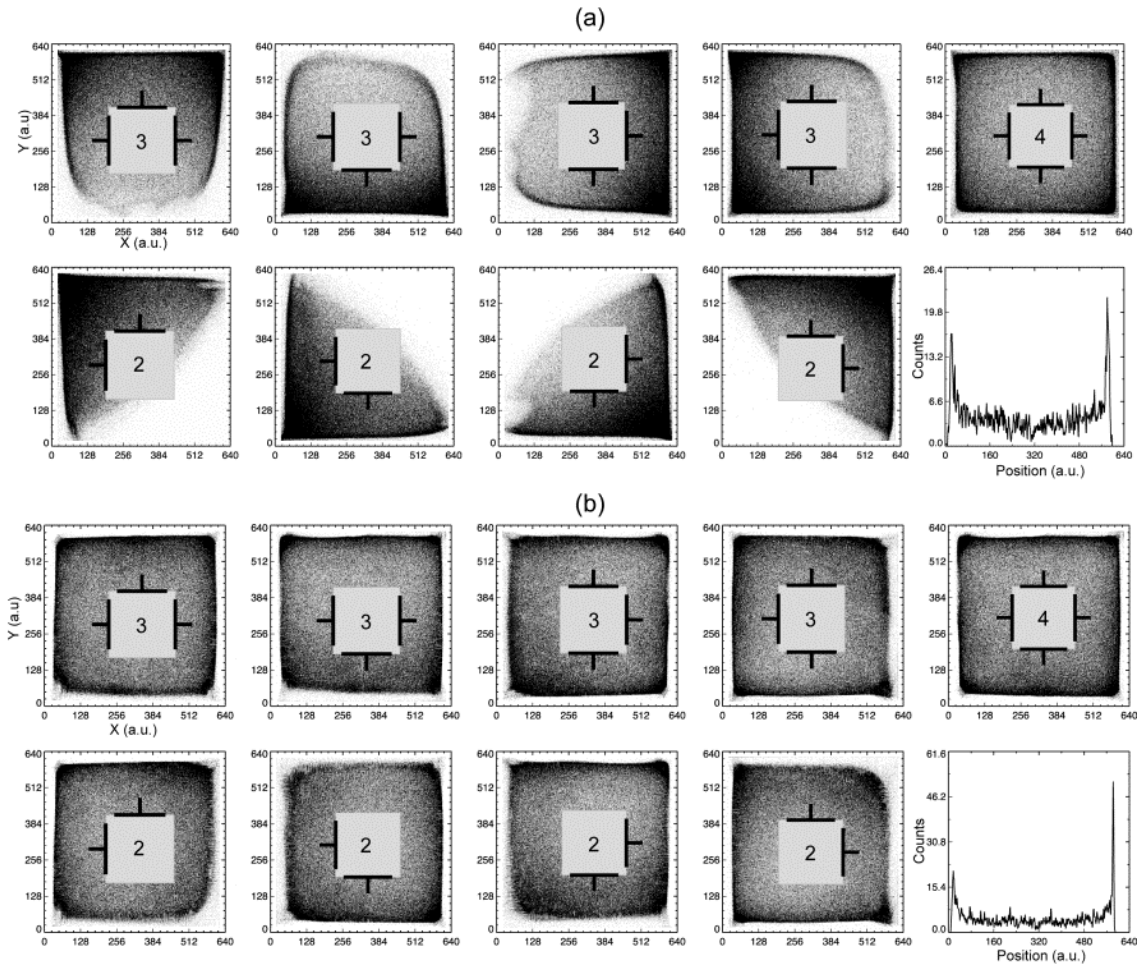

Fig. 8. 2D distributions of the photoabsorption events (counts) projected onto the X-Y plane evaluated for a representative detector using the linear (a) and second-order (b) approximation for the pads response functions. 9 maps from each group correspond to using different combinations of the signal amplitudes captured from the 4 pads. The specific pads whose signals were used to reconstruct the even locations are indicated in each map.

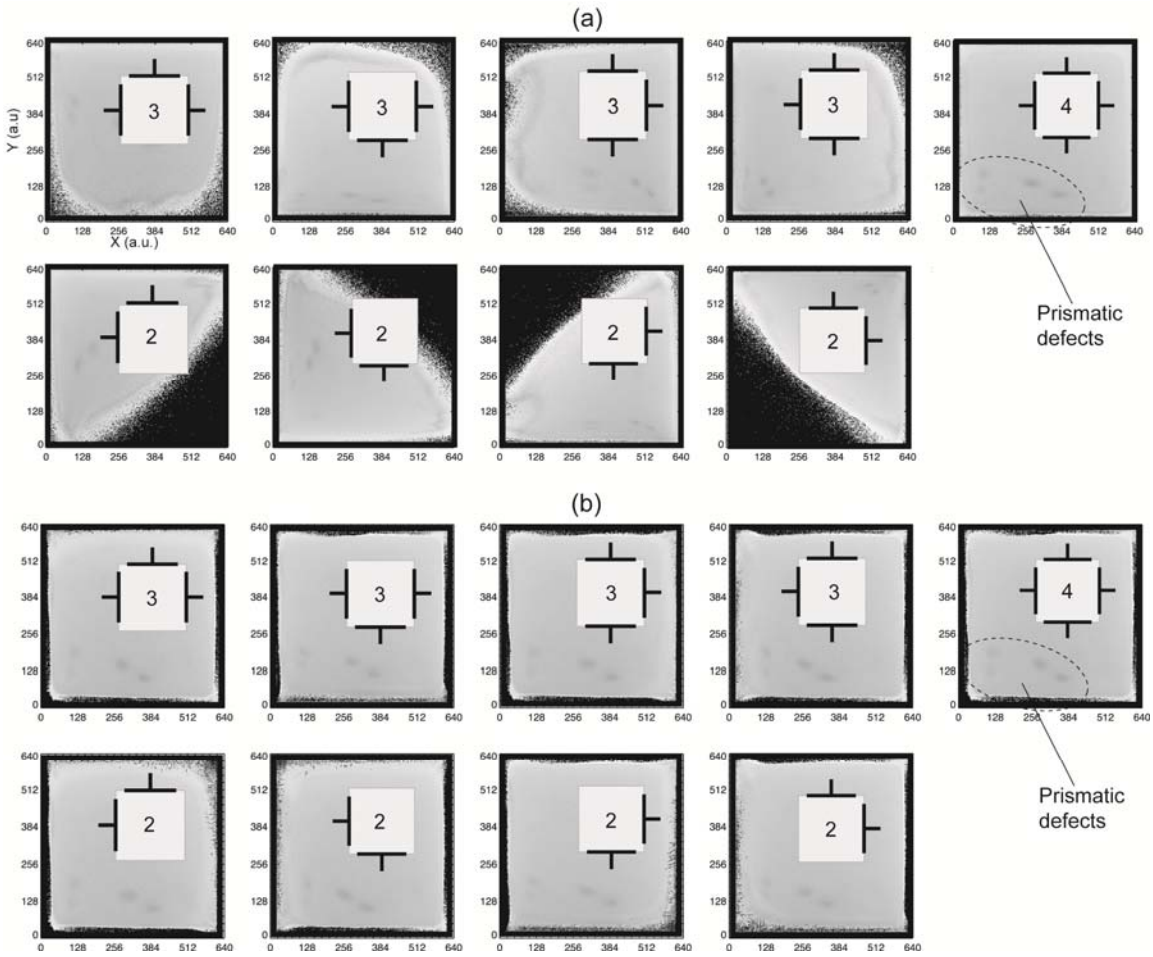

Fig. 9. Same as Fig. 8 but showing the response maps. The dark features are the prismatic defects in CZT (typical for Redlen material).

IV. Conclusions

We evaluated design approaches and performance of small, 2x2 and 3x3, VFG array prototypes coupled with a front-end ASIC. Our assessment focused on the expected energy and position resolutions of these arrays composed of commercial CZT crystals from eV Products and Redlen Technologies. The main factor limiting the energy resolution of the position-sensitive VFG detectors is electronic noise related to the high leakage current and large anode capacitance. Therefore 3D corrections played an important role to demonstrate the feasibility of position-sensitive VFG CZT detectors and arrays of such detectors for high resolution gamma-ray spectroscopic measurements.

We were able to achieve energy resolution of ~ 0.9% FWHM at 662 keV after corrections. To evaluate the actual *X-Y* locations of the interaction points inside the detector, we utilized the pads' response functions. We were also able to estimate the size of the smallest feature (prismatic defect) in the crystals to be less than 0.5 mm. This gives a good estimate for the *absolute* position resolution of the VFG detector with the charge-sensing pads. The *local* position resolution was approximately 100 μm.

These results demonstrate the feasibility of position-sensitive VFG CZT detectors and arrays of such detectors for high resolution gamma-ray spectroscopic measurements. After applying the 3D corrections, we achieved an energy resolution below 1% FWHM at 662 keV with a majority of the CZT crystals that we either grew at BNL or obtained from commercial suppliers. The ability to use the majority of CZT crystals should bring down the cost significantly making this design useful in the manufacturing of commercial detectors.

Although our results are very promising, the AVG1 ASIC was designed for different applications and is not optimal for VFG detectors. Use of the next-generation VGA ASIC with extended dynamic range and optimized shaping times for the pad signals will enable us to apply more accurate corrections.

References

[1] A. E. Bolotnikov, G. S. Camarda, Y. Cui, G. De Geronimo, J. Fried, A. Hossain, K. Lee, G. Mahler, M. Maritato, M. Marshall, M. Petryk, U. Roy, E. Vernon, G. Yang and R. B. James, "Use of high-granularity position sensing to correct response non-uniformities of CdZnTe detectors", Appl. Phys. Lett. 104, p. 263503, 2014.

[2] A. E. Bolotnikov, G. S. Camarda, E. Chen, S. Cheng, Y. Cui, R Gul, R. Gallagher, V. Dedic, G. De Geronimo, L. Ocampo Giraldo, J. Fried, A. Hossain, J. M. MacKenzie, P. Sellin, S. Taherion, E. Vernon, G. Yang, U. El-hanany and R. B. James, "CdZnTe Position-Sensitive Drift Detectors with Thicknesses Up to 5 cm", Appl. Phys. Lett. 108, p. 093504 (2016).

[3] V. V. Dmitrenko, A. C. Romanuk, Z. M. Uteshev, and V. K. Chernyatin, "Spectrometric applications of an ionization-type drift chamber", Pribory I Tekhnika Eksperimenta, vol. 1, pp. 51-53, 1982. Translation in Instruments and Experimental Techniques (USA), vol. 25, no. 1, pp. 50-53 (1982).

[4] K. Parnham, C. Szeles, K. G. Lynn, and R. Tjossem, "Performance Improvement of CdZnTe Detectors Using Modified Two-Terminal Electrode Geometry," in Hard X-ray, Gamma-Ray and Neutron Detector Physics, Proceedings of SPIE Vol. 3786, pp. 49-54, 1999.

[5] C. Szeles, D. Bale, J. Grosholz, Jr., G. L. Smith, M. Blostein, and J. Eger, "Fabrication of High Performance CdZnTe Quasi-Hemispherical Gamma-ray CAPture™ Plus Detectors", Hard X-Ray and Gamma-Ray Detector Physics VIII, edited by Larry A. Franks, Arnold Burger, and Ralph B. James, Proceedings of SPIE Vol. 6319 (SPIE, Bellingham, WA, 2006).

[6] D. S. McGregor and R. A. Rojeski, "High-resolution ionization detector and array of such detectors", US Pat. 6175120, 2001.

[7] G. Montemont, M. Arques, L. Verger, and J. Rustique, "A Capacitive Frisch Grid Structure for CdZnTe Detectors", IEEE Trans. Nucl. Sci. 48, pp. 278-281, 2001.

[8] A. E. Bolotnikov, K. Ackley, G. S. Camarda, C. Cherches, Y. Cui, G. De Geronimo, J. Fried, D. Hodges, A. Hossain, W. Lee, G. Mahler, M. Maritato, M. Petryk, U. Roy, C. Salwen, E. Vernon, G. Yang, and R. B. James, "An array of virtual Frisch-grid CdZnTe detectors and a front-end application-specific integrated circuit for large-area position-sensitive gamma-ray cameras," Review of Scientific Instruments, vol. 86, no. 7, 2015.

[9] G. De Geronimo, E. Vernon, K. Ackley, A. Dragone, J. Fried, P. O'Connor, Z. He, C. Herman, and F. Zhang, "Readout ASIC for 3-D position-sensitive detectors," IEEE Trans. Nucl. Sci., vol. 55, no. 3, pp. 1593–1603, 2008.

[10] E. Vernon, K. Ackley, G. De Geronimo, J. Fried, P. O'Connor, Z. He, C. Herman, and F. Zhang, "ASIC for high rate 3-D position sensitive detectors," IEEE Trans. Nucl. Sci., vol. 57, no. 3, pp. 1536–1542, 2010.

[11] F. Zhang, C. Herman, Z. He, G. De Geronimo, E. Vernon, and J. Fried, "Characterization of the H3D ASIC readout system and 6.0 cm^3 3-D position sensitive CdZnTe Detectors," IEEE Trans. Nucl. Sci. 59, pp. 236-242, 2012.

[12] A. E. Bolotnikov, J. Butcher, G. S. Camarda, Y. Cui, G. De Geronimo, J. Fried, R. Gul, P. M. Fochuk, M. Hamade, K. H. Kim, O. V. Kopach, M. Petryk, E. Vernon, G. Yang, and R. B. James, "Array of Virtual Frisch-Grid CZT Detectors With Common Cathode Readout for Correcting Charge Signals and Rejection of Incomplete Charge-Collection Events," IEEE Transactions on Nuclear Science, vol. 59, no. 4, pp. 1544-1551, 2012.